P7.6

# High-resolution numerical simulation of gravity wave-induced turbulence in association with an upper-level jet system

Chungu Lu[1†], William Hall[2], and Steven Koch[1]

[1] *NOAA Earth System Research Laboratory/ Global Systems Division*

[2] *National Center for Atmospheric Research*

## 1. Introduction

Clear-air turbulence (CAT) is frequently observed in the vicinity of upper-level jet streaks. Such turbulence generation coincides with the occurrence of gravity waves at approximately the same location – on the northeast side of the jet exit region. These observations point to a possible chain-reaction relationship between an upper-level jet, gravity waves, and CAT. However, an upper-level jet system, representing a synoptic-scale feature, typically possesses a scale on the order of several thousand kilometers, whereas gravity waves, as mesoscale phenomena, span scales from a few kilometers to a few hundred kilometers, and turbulence is categorized as a micro-scale feature whose spatial scale ranges from a few meters to a few hundred meters. Turbulence at atmospheric boundary layers is typically treated as subscale motions, and thus is parameterized in the atmospheric numerical models. CAT, on the other hand, is neither directly simulated nor parameterized in any of the typical atmospheric models.

In this study, we present simulations of CAT generation using a high-resolution numerical model with multi-nested domains. The simulation starts with a balanced upper-level jet. Mesoscale gravity waves are generated as a result of the intensification of tropospheric baroclinicity. These gravity waves experience scale contraction and eventually break, resulting in turbulent flow in the upper troposphere.

## 2. WRF model setup

The Weather Research and Forecast model (WRF, version 2.0) is used to simulate the entire process of generation of gravity waves and turbulence in association with a three-dimensional upper-level jet system in a baroclinically-unstable atmosphere. We initialize the WRF model with a PV-inverted baroclinic atmosphere with a uniform upper-level jet. In Fig. 1, we plot this initial state of atmosphere: a jet core of the zonal wind (color shaded) is located at about 9-10 km altitude, and a north-south temperature gradient exists in the lower atmosphere (isentropes).

Periodic lateral boundary conditions in the east-west direction and symmetric lateral boundary conditions in

*[† also in collaboration with Colorado State University]*

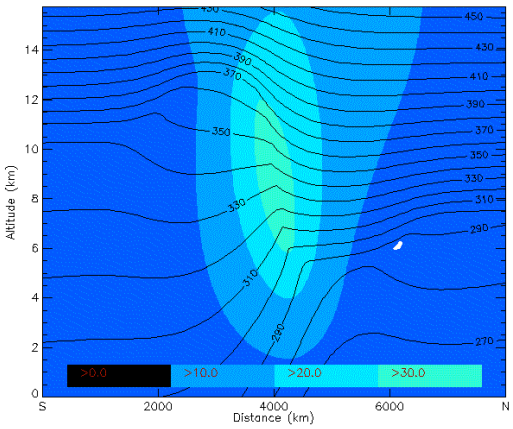


***Fig. 1:*** *The initial state of the idealized baroclinic atmosphere used in the WRF simulation shown in a vertical cross section normal to the jet axis. Contours are isentropes (contour interval every 10 K), color-shading shows isotachs of the zonal wind, representing the uniform upper-level jet (m $s^{-1}$). South is to the left.*

the north-south direction are used for the outer domain. In order for the simulated features to be stationary relative to the model domain, we developed a Galilean transformation for the model equations by first subtracting off a constant wind from the initial conditions, and then adding back the same amount of the wind to the Coriolis term in the model equations. We also adjusted the initial perturbation location so that the feature of interest is located in the center of the model domain.

Six one-way nested grids were employed in the model simulation. Each nested grid has different horizontal grid spacing, but keeps the same uniform vertical grid spacing, which is 250 m. The time step is adjusted for each nested domain according to spatial grid ratio in order for the CFL condition to be satisfied.

In order to simulate turbulence, we turn off all turbulence parameterization options in the model at the highest grid resolutions, and instead, we prescribe constant diffusion coefficients for both vertical and horizontal diffusion terms.

## 3. Simulated baroclinic wave and upper-level jet

The outer model domain (d1) is a rectangular domain with a dimension of 8000 km in the north-south direction, and 4000 km in the east-west direction. The grid spacing is 100 km. Fig. 2 shows the simulated upper level jet at a level of 9 km. One can see that within 24-h of WRF simulation time, the jet (color-shaded) and geopotential (labeled contour lines) fields show little change (panel a). On the fifth day (panel b), the jet and geopotential begin to show wavy structure, and by the seventh day (panel c), the jet intensifies to 50 m $s^{-1}$. By the final day of the model simulation (panel d), the mature jet begins to split and break down.

This evolution of the upper-level jet system is a response to the tropospheric baroclinic development. In order to see this, we plot surface pressure (contours) and potential temperature (color-shaded) fields in the corresponding times in Fig. 3. Panel a clearly shows a prelude of developing baroclinic waves (a weak high and low system). The low system intensifies through the fifth day, at which time an occluded region has developed (panel b). By the seventh day (panel c), the temperature gradient has intensified rapidly with the further intensification of the low center, and this development continues into the final model time, the ninth simulation day shown in panel d.

## 4. The banded structure of divergence and mesoscale gravity waves

With the successful simulation of the synoptic environment, we now wish to examine the mesoscale development in response to this synoptic dynamical evolution. To do this, we designed a second domain (d2) nested inside the outer domain. We positioned the nested domain on the northeast side of the exit region of the upper level jet (see Fig. 2c-d) since we are interested in the possible generation of turbulence, which we expect to be most likely in this region as the jet approaches the intensifying upper-level ridge axis (Uccellini and Koch 1987). The nested domain constitutes a rectangular domain of 2000x3000 km. The grid spacing for this domain is 20 km. The integration of this domain starts at 12:00 h on the fifth day of the outer domain integration. Since the mesoscale motions are most likely to develop in response to the unbalanced flow of the large-scale forcing, we concentrated on the divergence field in the left exit region of the upper level jet. Fig. 4 shows the divergence field (image) and jet location (color shaded) at 12-km altitude.

Because many observational studies indicate that clear-air turbulence tends to occur in the region near the upper-level ridge as the jet is approaching the ridge line, we designed our third domain to be nested inside the second domain in this relative location, as shown in Fig. 4. One can see that the divergent flow increases with time within this sub-domain and tends to form banded structures.

The third domain (d3) is a square domain with a size of 800x800 km and a grid spacing of 4 km. The simulation of flow in this domain starts at 0 h on the seventh day. In order to see whether the banded divergence field is related to the generation of mesoscale gravity waves, we plotted the divergence by hatching and upward vertical velocity as image-field at 12-km height in Fig. 5a-b. The two fields are correlated very well, and both present the strong appearance of mesoscale wave structure. Mesoscale gravity waves can be identified with scales (horizontal wavelength) of ~150-400 km (Fig. 5a). As time increases, superimposed on these waves, many small-scale features are generated (Fig. 5b). This picture can also be seen in the vertical cross-section plots for the same time (at time 153 and 159 h) along the black cross lines (Fig. 6). It seems from Fig. 6 that the mesoscale waves can be traced to the surface divergence structure related to the development of the baroclinic wave, and that these waves have a slightly vertical propagation component. On the other hand, the small-scale features are presented as very fine internal waves, and they tend to propagate horizontally and towards the southwest (not shown; identified by taking a frequent time sequence).

## 5. Generation of small-scale gravity waves

To examine even smaller-scale internal waves superimposed on the mesoscale gravity waves, we established the fourth nested domain (d4) with a size of 200x200 km and a grid resolution of 1 km (the box on Fig. 5a-b). This domain is initialized at 6h on the seventh day. The vertical velocity field does present a

set of small-scale gravity waves with wavelength varying between 10-30 km (Fig. 7a,b). As these waves propagate to the southwest, they appear to become more pronounced at later times and generate a plume of turbulent, chaotic flow (Fig. 7c). The generation of small-scale, internal gravity waves is believed to be due to wave-wave interaction of mesoscale gravity waves appeared in d3 (Fig. 5). The idea that the nonlinear advection terms in the Navier-Stokes equation can generate higher wavenumber harmonics from the dominant wave has been put forward in Weinstock (1986). Lu et al. (2005) also presented a study of wave scale contraction using two-dimensional spectral analysis and wavelet-based Hovmoller diagrams. The generation of secondary waves due to wave-wave interaction has been studied in Kuo et al (1999) and Krishan and Selim (1968). However, we have not yet determined why turbulence is generated in this particular part of the overall flow pattern. Also, numerical issues related to possible wave reflection in the lateral boundary zones are currently being analyzed very carefully to ensure that this wave-turbulence interaction is being depicted entirely physically and cannot be attributed to numerical noise.

We further nested down to a higher-resolution domain with a finer time sequence to see what happen for these internal gravity waves. Domain d5 has a size of 100x100 km and the grid spacing for this domain is 500 m. Fig. 8a-d plots a 40-minute sequence of the lower corner of d4 between the time 158:40 to 159:10 (see box on Fig. 7b). One can see that these waves became resolved at ~159:00 and generated small-scale eddies.

## 6. Wave breaking and turbulence generation

We use the sixth nested domain (d6) in an attempt to animate the complex process by which the gravity waves break and turbulence is generated. Domain d6 covers a 50x50 km area with grid spacing of 250 m. The vertical velocity (image) and the geopotential height (white contours) are plotted every 2 minutes (Fig. 9). It can be inferred how one branch of the waves breaks and turbulence results. When turbulence is generated, the geopotential fields lose their organized structure, indicative of the occurrence of strong mixing by turbulent flows. However, the complexity of this process is overwhelming and will require more sophisticated three-dimensional visualization of the evolving flow pattern to be able to gain a deeper understanding of these processes.

## 7. Conclusions

We have presented a high-resolution WRF model simulation of the development of an upper-level jet, baroclinic waves, mesoscale gravity waves, wave scale contraction, wave breaking, and generation of turbulence. This modeling effort covers nearly the entire atmospheric energy spectrum, including synoptic scale, mesoscale, micro-scale to dissipation range. Since we used the multi-nesting utility in the WRF modeling system, all these different-scale atmospheric features can be dynamically linked together and simulated with successive local refinement.

Although the simulations presented in this study give reasonable results and can be used for understanding the scale interaction of the physical processes concerned here, these are very preliminary results. More detailed and quantitative analyses are still in progress, including thorough study of numerical stability and boundary condition issues, improved means for displaying the complexity of wave-turbulence interactions, a theoretical study of the normal modes of the simulated atmosphere, and deeper understanding of what conditions are necessary and sufficient for gravity waves to produce moderate-or-greater turbulence levels

***Acknowledgments***: We would like to thank Dr. Ligia Bernardet, who conducted the NOAA internal review, and Susan Carsten, who conducted technical editing. This research is in response to requirements and funding by the Federal Aviation Administration (FAA). The views expressed are those of the authors and do not necessarily represent the official policy or position of the FAA.

**References**

Krishan S., and A. Selim, 1968: Generation of transverse waves by non-linear wave-wave interaction. *Plasma Phys.,* **10**, 931-937.

Kuo, F., C. Lo, H. Lue, and C. Huang, 1999: A study of secondary waves generated by wave-wave interaction in a wind field. *Chinese J. Phys.,* **37**, 240-257.

Lu, C., S. Koch, F. Zhang, and N. Wang, 2005: Modeled mesoscale gravity waves: Continuous spectrum and energy cascade. *11th Conf. on Mesoscale processes*, Albuquerque, NM, Amer. Meteor. Soc.

Uccellini, L. W., and S. E. Koch, 1987: The synoptic setting and possible energy sources for mesoscale wave disturbances. *Mon. Wea. Rev.,* **115,** 721–729.

Weinstock, J., 1986: Finite amplitude gravity waves: Harmonics, advective steepening and saturation. *J. Atmos. Sci.,* **43,** 688–704.

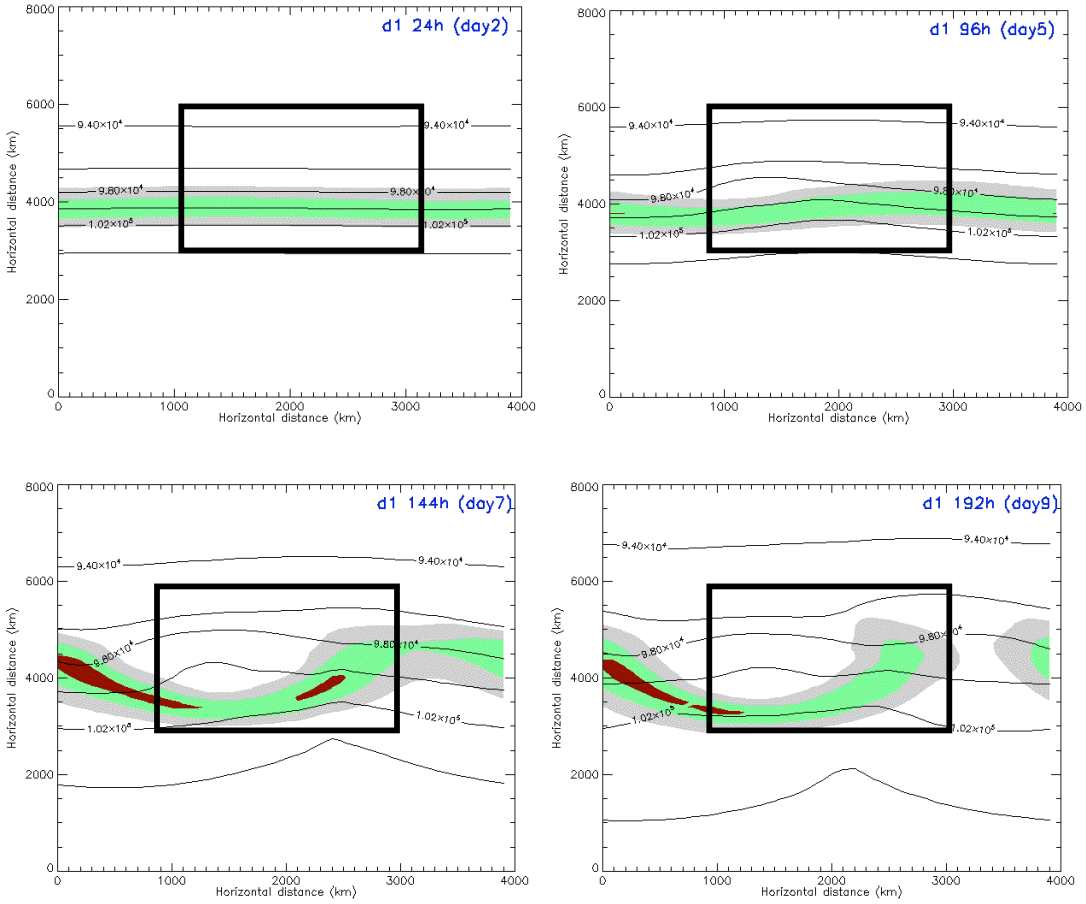


***Fig. 2:*** *WRF model simulation of the upper-level jet at 9-km altitude (color-shaded). Isotachs of 30 m $s^{-1}$ (grey), 40 m $s^{-1}$ (green), and 50 m $s^{-1}$ (red) are displayed, at day 1, 5, 7, and 9 for the outer (d1) domain. The contours are geopotential fields. The boxes in each figure panel show the nested domain (d2).*

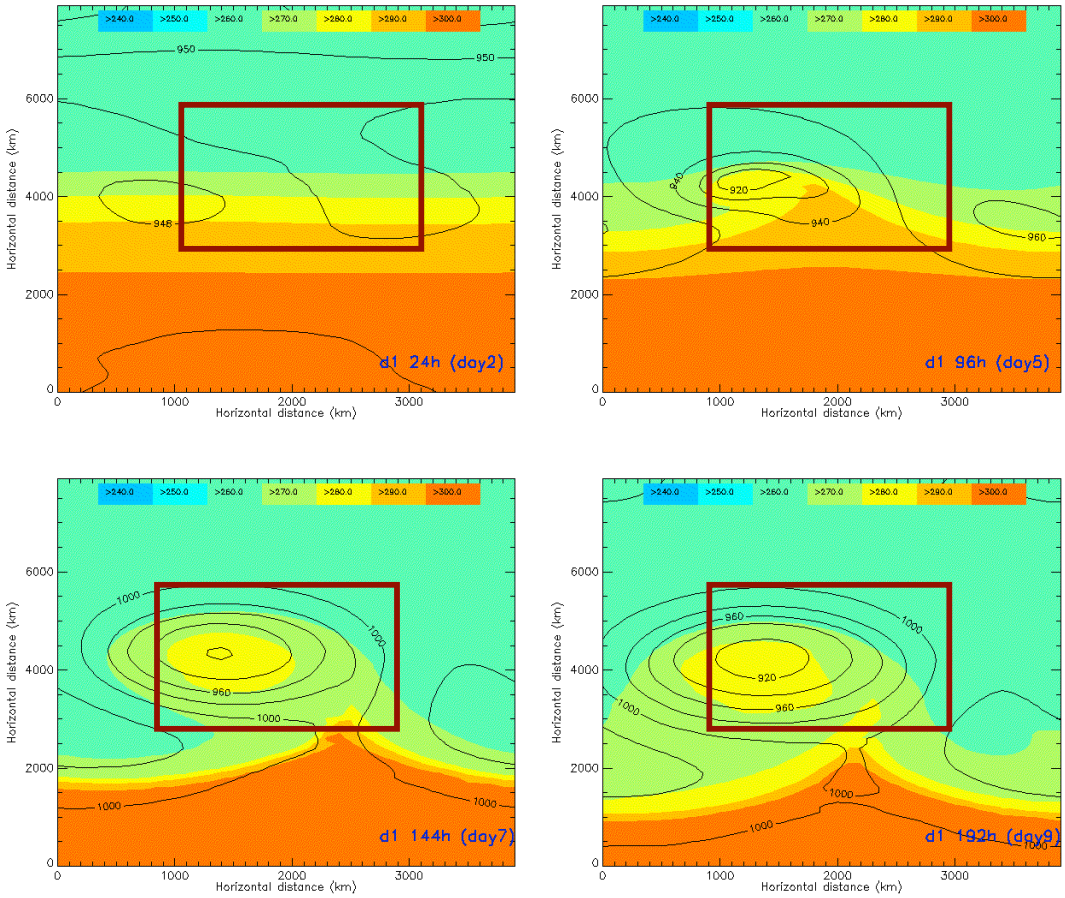


***Fig. 3:*** *WRF model simulation of baroclinic waves at day 1, 5, 7, and 9 for the outer domain (d1). The color-shaded fields are surface potential temperature, and the contours are surface pressure. The boxes in each figure panel show the nested domain (d2).*

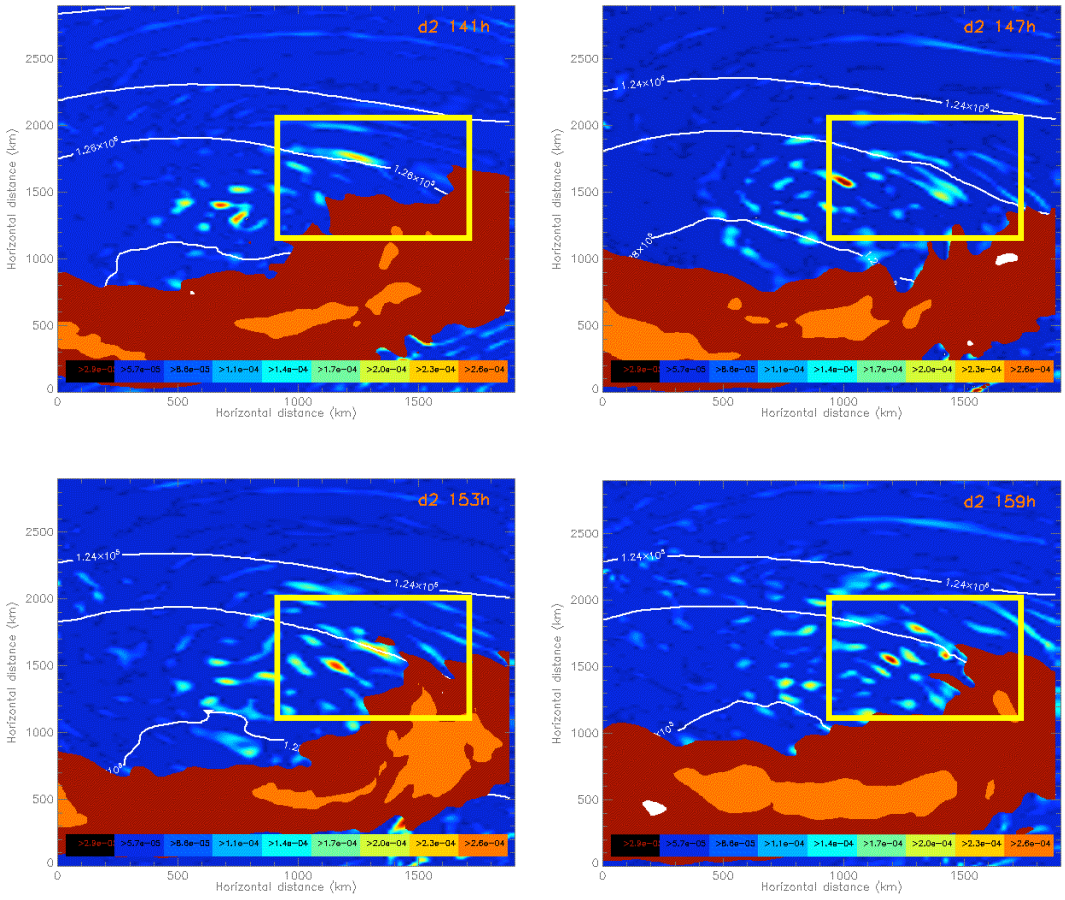


***Fig. 4:*** *Divergence (color shading), geopotential, and the upper-level jet (isotachs shown by broad swath of reddish imagery near the southern border) at 12-km altitude in domain d2 at 141, 147, 153, and 159 h. The boxes in each figure panel show the nested domain (d3).*

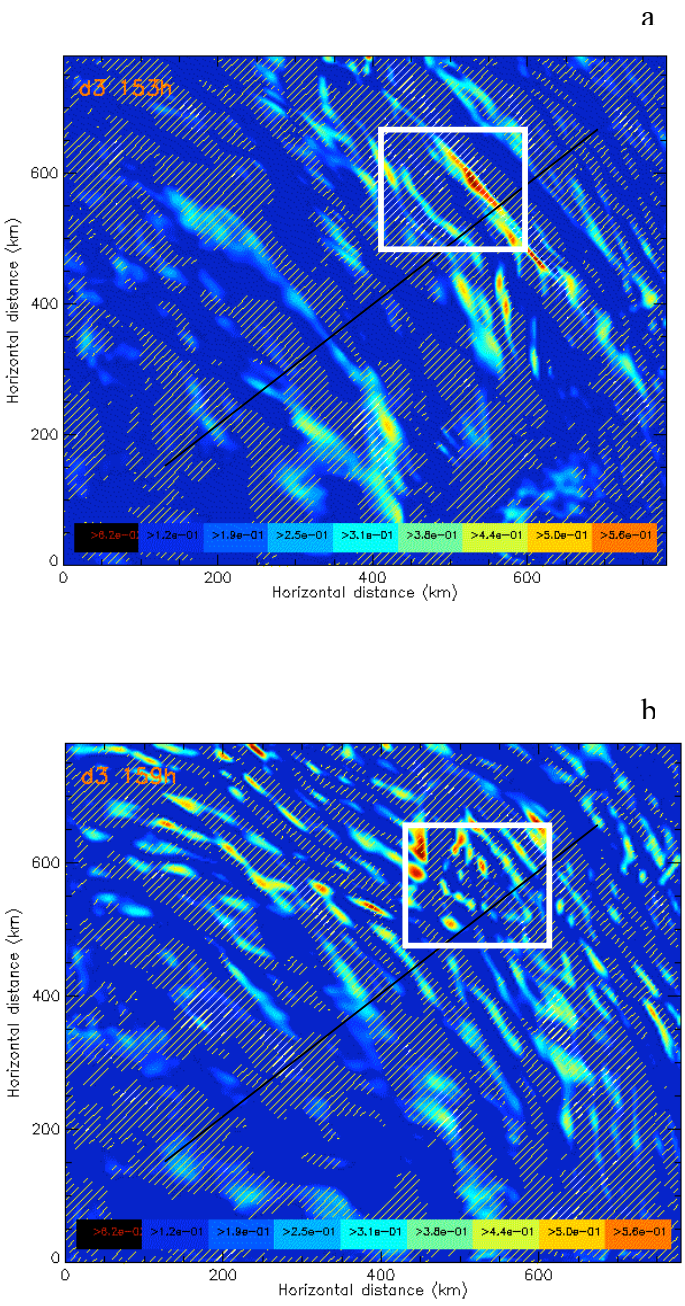


***Fig. 5:*** *Divergence (line-shaded) and vertical velocity (image) at 12-km altitude in domain d3: a) at 153 h; and b) at 159 h. Black lines indicate the vertical cross-section shown in Fig. 6. The white boxes are the location of the nested domain (d4).*

a

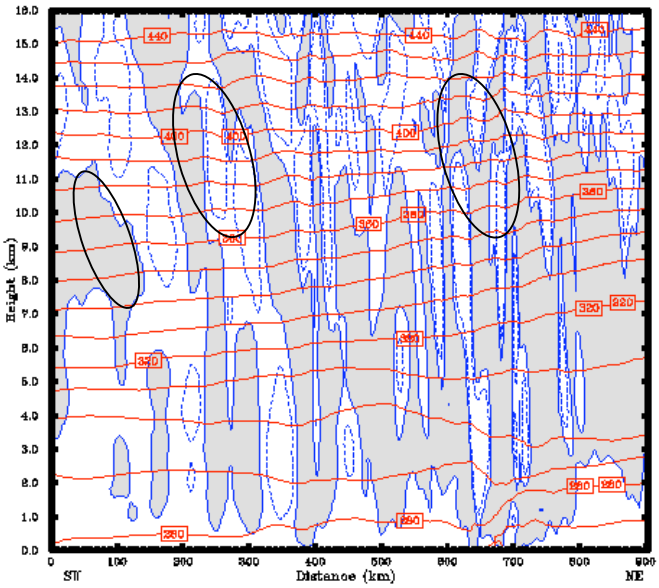


b

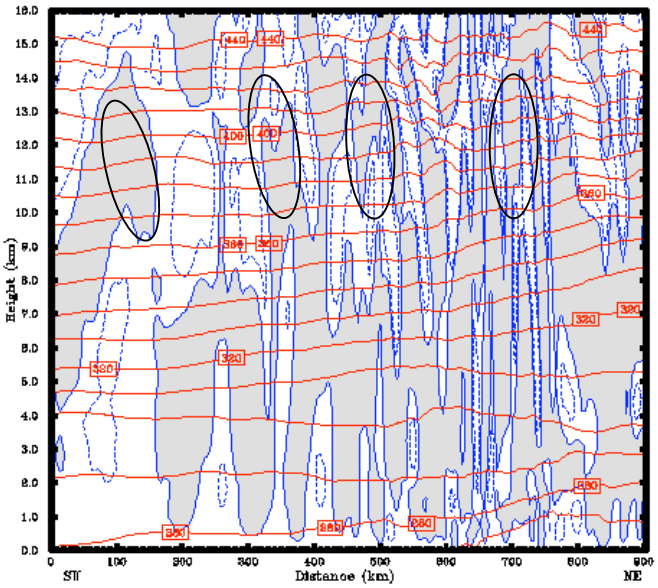


***Fig. 6:*** *Vertical cross-section view of vertical velocity (shaded grey) and potential temperature (red contours) along black lines in Fig. 5: a) at 153h; b) at 159h. The elliptic shapes indicate the locations of mesoscale gravity waves.*

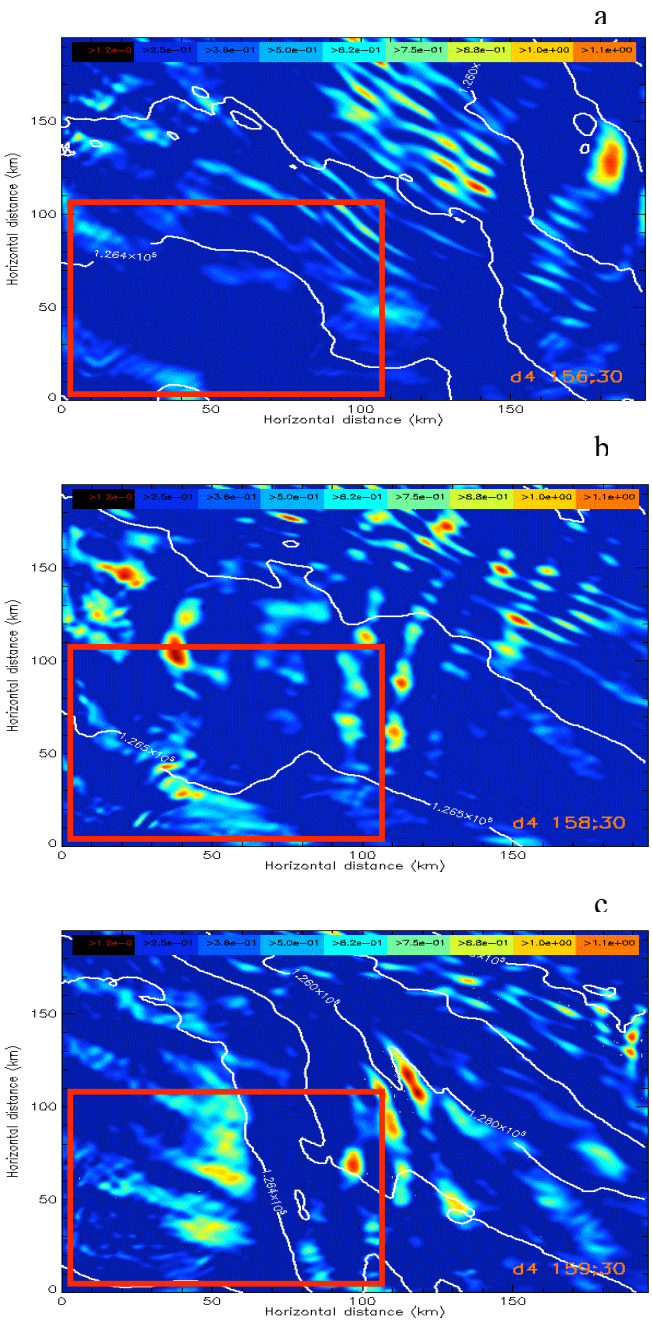


***Fig. 7:*** *Vertical velocity (image) and geopotential (white contours) at 12-km altitude for domain d4: a) at 156:30; b) 158:30; and c) 159:30. The boxes show the location of domain d5.*

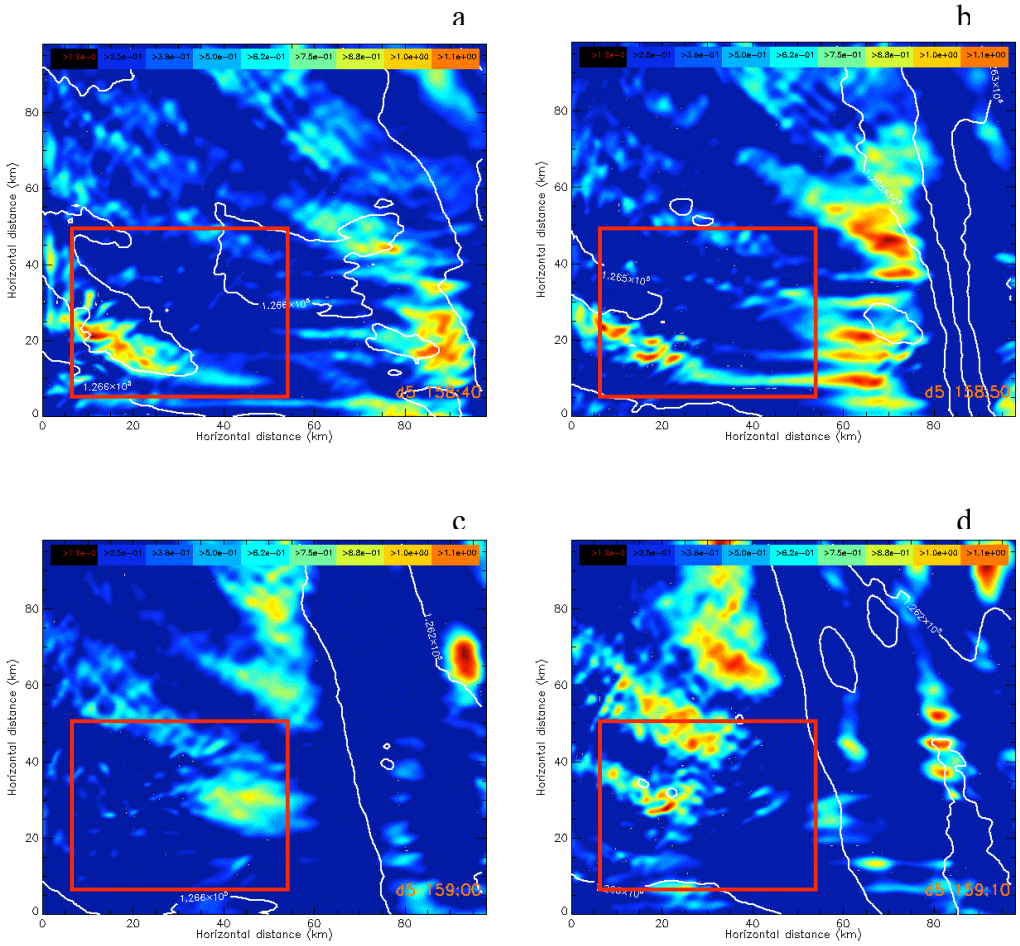


***Fig. 8:*** *Vertical velocity (image) and geopotential fields (white contours) at 12-km altitude for domain d5: a) at 158:40; b) at 158:50; c) at 159:00; and d) at 159:10. Red boxes indicate the location of the nested domain d6.*

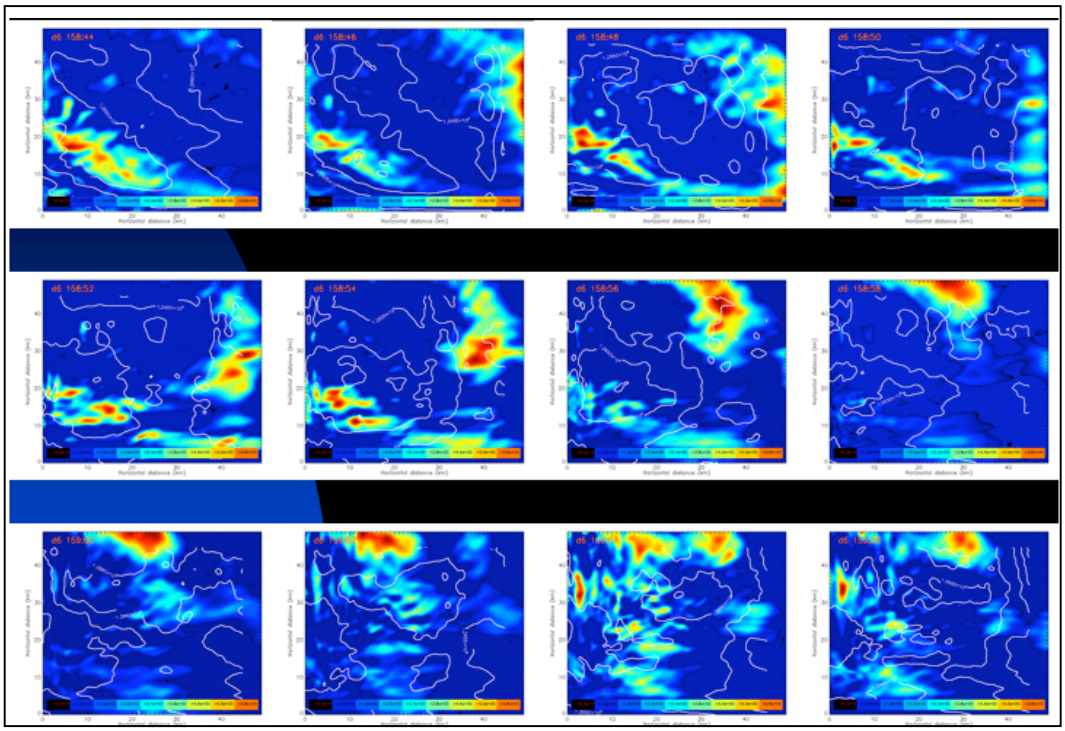

***Fig. 9:*** *Vertical velocity (image) and geopotential (white contours) at 12-km altitude for domain d6. The animation starts with time at 158:44 and ends at 159:06 with 2 minutes between each frame (time increases left to right, then down).*